Supplementary Information (SI) for Journal of Materials Chemistry A.
This journal is © The Royal Society of Chemistry 2024

Supplementary information

LED-driven Hematite/$Bi_4O_5I_2$ nanocomposite as S-scheme heterojunction photocatalyst for efficient degradation of phenolic compounds in real wastewater

Akash Rawat [a], *Suneel Kumar Srivastava* [b,δ], *Chandra Sekhar Tiwary* [c],

Ashok Kumar Gupta [d,*]

[a] School of Environmental Science and Engineering, Indian Institute of Technology Kharagpur, Kharagpur 721302, India

[b] Department of Chemistry, Indian Institute of Technology Kharagpur, Kharagpur 721302, India

[c] Metallurgical and Materials Engineering, Indian Institute of Technology Kharagpur, Kharagpur 721302, India

[d] Environmental Engineering Division, Department of Civil Engineering, Indian Institute of Technology Kharagpur, Kharagpur 721302, India

* Corresponding author

E-mail address: agupta@civil.iitkgp.ac.in

[δ] Former faculty member of the Department of Chemistry, Indian Institute of Technology Kharagpur, Kharagpur 721302, India

S1. Materials and chemical reagents

For synthesis of photocatalyst: Hematite ore (acquired from the Department of Mining, IIT Kharagpur) Bismuth (III) nitrate pentahydrate ($Bi(NO_3)_3 \cdot 5H_2O$; ≥ 99% purity), Potassium iodide (KI; ≥ 99% purity), Ethylene glycol ($C_2H_6O_2$; ≥ 99% purity), Sodium hydroxide (NaOH; ≥ 99% purity, Hydrochloric acid (HCl; 35%), Ethanol (C_2H_5OH; ≥ 99.9%). For the study of the influence of co-existing anions: Sodium chloride (NaCl; ≥ 99.5% purity), Sodium carbonate (Na_2CO_3; ≥ 99.5% purity), Sodium dihydrogen phosphate (NaH_2PO_4; ≥ 99.99% purity), Sodium bicarbonate ($NaHCO_3$; ≥ 99.5% purity), Sodium nitrate ($NaNO_3$; ≥ 99.9%), and Sodium sulphate anhydrous (Na_2SO_4; ≥ 99% purity). For radical scavenging studies: Ascorbic acid ($C_6H_8O_6$; ≥ 99.9%), Silver nitrate ($AgNO_3$), and 2-propanol (C_3H_8O; ≥ 99.99% purity). For immobilization: Polyvinyl alcohol (PVA). *Phenolic compounds used in this study: Bisphenol A ($(CH_3)_2C(C_6H_4OH)_2$; ≥ 99% purity), m-cresol (C_7H_8O; ≥ 99% purity), phenol (C_6H_5OH; ≥ 99% purity). All of the chemicals were used in analytical grade without further purification and purchased from Merck India.

*Preparation of stock solution

0.1 g of Phenolic compound (BPA or m-cresol A or Phenol) was dissolved in 1000 mL DI water and stirred until completely dissolved. After that, the prepared stock solution of 100 mg/L was kept in the dark ambiance at -4 ºC and diluted according to the experimental requirements.

S2. Characterization techniques

The samples' surface morphology was analyzed using high-resolution (FEG-SEM) on Zeis Merlin Gemini II at an accelerating voltage of 20 kV. The structure and composition of the material were examined using 200 kV high-resolution transmission electron microscopy (HR-TEM) on Talos F200X G2, Thermo Scientific. The XRD patterns of each synthesized material were recorded using

a Malvern PANalytical X'Pert Powder diffractometer with Cu Kα radiation (λ = 0.154 nm) at a scanning rate of 5° 2θ per minute. The 3D profile, topographical, and textural features, including roughness parameters (as per ISO 25178), were obtained from atomic force microscopy (AFM) images recorded using an Agilent 5500 atomic force microscope. The XPS of the material, indicating the available orbital states, was recorded using a PHI 5000 VersaProbe III (ULVAC PHI, Physical Electronics, USA) equipped with a monochromatic Al Kα X-ray source and a focused beam adjustable from <10 μm to 300 μm for rapid X-ray-induced secondary electron imaging (SXI). The system includes a 180° hemispherical electron energy analyzer with a 128-channel detector, an argon ion gun (0-5V) for specimen cleaning, depth profiling, and charge neutralization, and a Gas Cluster Ion Beam (GCIB) (2.5-20 kV Ar) for low-damage surface cleaning. Sample heating and cooling capabilities range from 800 ºC to -140 ºC. The work function of each material was determined using ultraviolet photoelectric spectroscopy (UPS) and recorded on PHI 5000 VERSA PROBE III (energy source He I). The Brunauer-Emmett-Teller (BET) specific surface area, Barrett-Joyner-Halenda (BJH) pore volume, and nominal pore size were measured using nitrogen adsorption-desorption on an Autosorb iQ Station 1. Prior to analysis, the samples were degassed at 200 ºC under vacuum conditions. Photoluminescence PL spectra were obtained from F-4600 fluorescence with an excitation wavelength of 320 nm. UV–visible diffuse reflectance spectroscopy (UV-DRS) was performed from 300 to 800 nm using a Cary 5000 UV-Vis-NIR spectrophotometer equipped with an integrating sphere of diameter 150 mm, and band gap energies were determined by drawing a Tau plot. The Zeta potential of the nanocomposite was analyzed by ZS90 (Malvern Nano Zetasizer). The leaching of Fe and Bi ions was measured by multi-elemental scans using ICP-MS (iCAP PRO, Thermo Scientific, USA). The intermediates of phenolic compounds after certain intervals were identified by LC-MS/MS (WATERS 2695, USA)

S3. Experimental setup and procedure

A lab-scale photocatalytic reactor was developed by integrating several components, including a visible lamp (Lumina 50 Watts LED, 6500 K cool daylight with a luminous flux of 105 lm/w), a magnetic stirrer (Tarsons digital spinnot) with a bead, glass beakers with capacities of 200 mL and 1000 mL, and a box.[1] A white LED light was held 10 cm above the inner beaker of the jacketed beakers. The inner chamber contained the reaction suspension, while the outer beaker facilitated water circulation to provide cooling, maintaining the suspension's temperature at 25 ± 5 ºC. For the immobilized photocatalyst experiments, however, all tests were conducted in a 100 mL beaker without any cooling provisions.

The concentrations of phenolic compounds in suspension were analyzed using HPLC (Thermo Fisher Scientific, Ultimate 3000). A reverse phase C18 column measuring 4.6 cm × 250 mm was employed. The mobile phase consisted of a mixture of acetonitrile and deionized water in a 60:40 (V/V) ratio, with a detection wavelength set at 270 nm. The flow rate was kept constant at 1 mL/min, allowing for the detection of BPA, m-cresol, and phenol at retention times of 4.0, 4.53, and 5.2 minutes, respectively. Furthermore, the degradation efficiency and apparent rate constant was measured using the procedure given in our previous study.[1]

S4. Procedure for antibacterial assay

The toxicity assessment of the as-synthesized HBI-30 nanocomposite was conducted using the agar well diffusion test. The same procedure was followed as outlined in the study of [1–4]. Briefly, the investigations used pure strains of water pollution bioindicator Escherichia coli (ATCC 8739). After sterilization, nutritional agar was cooled on a flat surface. Fresh overnight E. coli cultures were evenly dispersed using a sterile cotton swab after agar plate solidification. Agar in each Petri plate was 6 mm thick. After that, three wells (~6 mm dia.) were cut from the agar plate. The first

well had 20 µL of Levofloxacin (positive control), the second well had 20 µL of DI (negative control), and the other wells housed 0.5 g/L HBI-30 nanocomposite solutions. After 10 min of diffusion, the agar plate was incubated at 35 °C for 24 h, and the zone of inhibition around the well was determined.

A conventional plate count test utilizing CFU count was performed to evaluate the toxicity of aqueous BPA before and after photocatalytic treatment. The sample included 10 mg/L BPA, 5 mg/L m-cresol and 5 mg/L phenol. Nutrient agar was prepared (suspend 28 grams in 1000 mL DI water and heat to boiling to dissolve the medium completely) and sterilized (autoclaving at 15 lbs pressure and 121 ^{o}C for 15 minutes), then 0.1 mL of the E. coli solution was spread on a Petri dish using the spread plate method. The CFU was counted after incubating the Petri plate at 35 °C for 24-48 h. This approach reveals PCs's potential toxicity and microbiological responses to it.

S5. Topographical features of HBI-30 nanocomposite

Table S1 presents the AFM surface roughness parameters, emphasizing the variations among the catalysts (Hematite, $Bi_4O_5I_2$, pristine HBI-30, and reused HBI-30). The low Sq value (0.645 nm), combined with the high Ssk (29.9) and Sku (1456) of Hematite, indicates a surface that is relatively smooth, which may limit photocatalytic activity.[5] In contrast, $Bi_4O_5I_2$ exhibits a higher value of sq (6.84 nm), suggesting rough surface characteristics that may enhance photocatalysis by offering a more active site. [1] The pristine HBI-30 nanocomposite heterojunction showcased a stable surface profile of 5.97 nm Sq, with notably reduced Ssk (7.79) and Sku (90.2), implying a smoother and more homogeneous surface that is advantageous for electron-hole separation. Furthermore, the HBI-30 photocatalyst, which was reused 10 times, demonstrated an increase in surface roughness with a Sq of 10.7 nm, suggesting agglomeration or degradation. Nevertheless, reused HBI-30 preserved Ssk (10.3) and Sku (142) values, indicating a stable surface that makes it acceptable for

extended photocatalytic uses regardless of minor changes in roughness parameters. The findings align with the BET analysis and are clearly illustrated in Fig. S3a-c.

S6. Photocatalytic degradation of m-cresol and phenol

Fig. S8a shows the photodegradation of *m*-cresol at varying initial concentrations (1–50 mg/L) while keeping other parameters constant (HBI-30 dose = 0.5 g/L, pH = 6.75, and irradiation time = 80 min). Up to 20 mg/L *m*-cresol, the degradation efficiency reached 100% but decreased to around 71% at 50 mg/L concentration. Similarly, for phenol, 100% degradation was observed at 1 mg/L concentration, which subsequently decreased to 35% at 50 mg/L (Fig. S8b).

S7. Source and characteristics of various water matrices

To examine the simultaneous photodegradation of PCs in different real water matrices, the water samples were collected from the following sources: tape water - School Environmental Science and Engineering, IIT Kharagpur (India), pond water - pond located in IIT Kharagpur campus (India), river water - Tangsawati river, West Bengal (India), and secondary treatment effluent - Sewage treatment plant, IIT Kharagpur (India). The characteristics of real water matrices are listed in Table S1.

Table S1. Surface roughness parameters for Hematite, $Bi_4O_5I_2$, HBI-30 (pristine), and HBI-30 (reused).

Parameters* / Catalyst	Root mean square height (Sq, nm)	Skewness (Ssk)	Kurtosis (Sku)	Maximum peak height (Sp, nm)	Maximum pit height (Sv, nm)	Maximum height (Sz, nm)	Arithmetic mean height (Sa, nm)
α-Fe_2O_3	0.645	29.9	1465	51.1	4.50	55.6	0.231
$Bi_4O_5I_2$	6.84	18.5	435	243	21.7	265	1.16
HBI-30 (Pristine)	5.97	7.79	90.2	121	72	193	1.88
HBI-30 (reused)	10.7	10.3	142	241	40.6	282	3.04

** Where, Sq signifies the standard deviation of surface height variation, Ssk quantifies the asymmetry of the surface profile, Kurtosis represents the sharpness of the surface peaks and valleys, Sp denotes the height of the highest peak from the mean plane of the surface, Sv indicates the deepest valley from the mean plane of the surface, Sz is the total profile height (the sum of Sv and Sp), and Sa measures the average deviation of surface height from the mean plane, commonly utilized to assess surface roughness*

Table S2. BET and BJH results of Hematite, $Bi_4O_5I_2$, and HBI-30.

Catalyst	SSA (m^2/g)	Pore volume (cc/g)	Average pore radius (Å)
Hematite	18.73	0.01732	18.50
$Bi_4O_5I_2$	43.43	0.02874	20.25
HBI-30	30.01	0.04031	19.12

Table S3. Characteristics of various water matrices.

Parameters	**DI water**	**Tap water**	**Pond**	**River water**	**Secondary treatment effluent**
pH	6.75 ± 0.15	7.2 ± 0.15	6.62 ± 0.15	6.55 ± 0.5	6.8 ± 0.2
Turbidity (NTU)	BDL	0.25 ± 0.1	11.5 ± 0.3	9.6 ± 0.3	40.8 ± 0.5
TSS (mg L^{-1})	BDL	5 ± 0.4	35 ± 0.4	32.5 ± 0.5	31 ± 0.4
TDS (mg L^{-1})	BDL	115 ± 5	178 ± 0.5	155 ± 0.5	305 ± 0.5
Chloride (Cl^-, mg L^{-1})	BDL	11.5± 1	29.02 ± 0.6	7.8 ± 0.05	49.6 ± 0.6
Bicarbonate (HCO_3^-, mg L^{-1})	BDL	21.2 ± 2	125 ± 1	145 ± 2	106 ± 0.2
Sulpahte (SO_4^{2-}, mg L^{-1})	BDL	2.9 ± 1	25.2 ± 0.8	4.1 ± 1	2.6 ± 0.2
Nitrate (NO_3^-, mg L^{-1})	BDL	BDL	54.2 ± 0.9	3.11 ± 0.2	5.75 ± 0.2
COD (mg L^{-1})	BDL	BDL	112 ± 0.12	62.5 ± 2	40 ± 2

Table S4. Degradation products formed and identified in LC-MS/MS.

Sr. No.	Degradation product	Compound	M/Z	Structure	Ref.
I		BPA	228	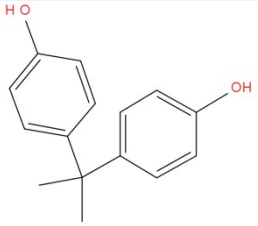	1,6
II		m-cresol	109	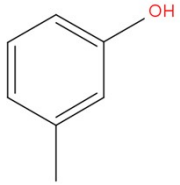	7,8
III		Phenol	94	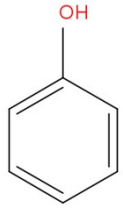	9,10
1.	A	5-Hydroxybisphenol	244	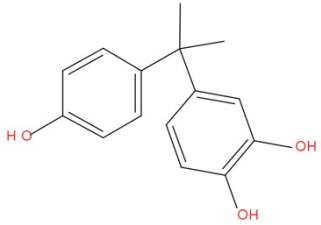	1,11

2.	A1	257	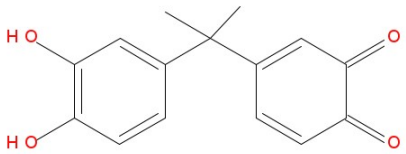	1,12,13
3.	A2	242	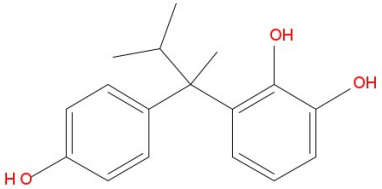	1,11
4.	A3	260	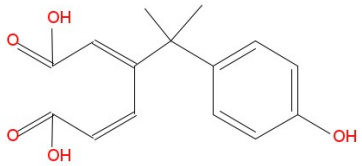	1,14
5.	A4	257	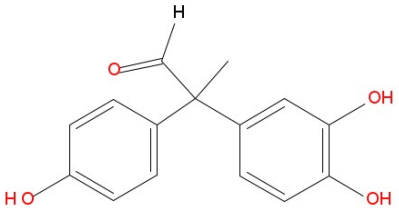	1,12,14,15
6.	A5	168	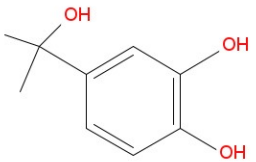	1,14
7.	A6	217	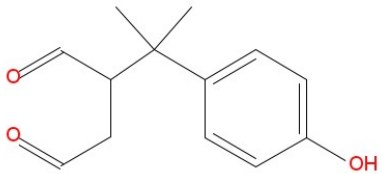	1,14

8.	A7		261	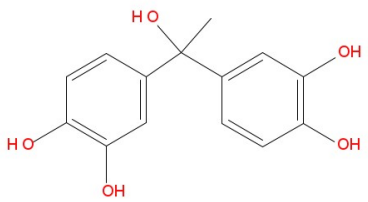	1,15,16
9.	B	2-methoxybenzene-1,4-diol	141	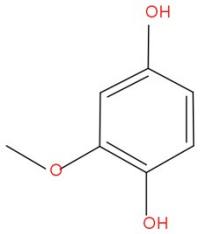	17
10.	B1	Benzene-1,4-diol or p-Dihydroxybenzene (Hydroquinone) (C6H6O2)	110	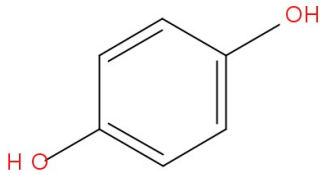	6,9,14,17
11.	C	4,4'-(1-Methyl-1,2-ethenediyl)bis[phenol]	226	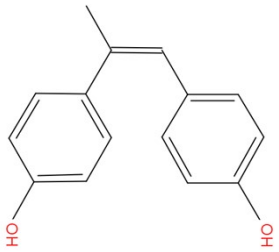	1
12.	C1		154	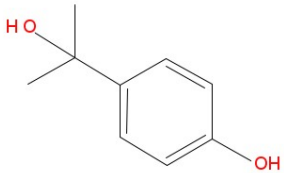	17,18

13.	C2	4-(Prop-1-en-2-yl)phenol	134	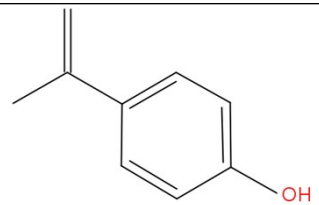	1,11,14,15
14.	C3	4-Hydroxyacetophenone	136	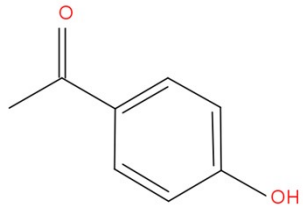	1,11
15.	C4	(4-(prop-1-en-2-yl)cyclohexa-3,5-diene-1,2-dione	147	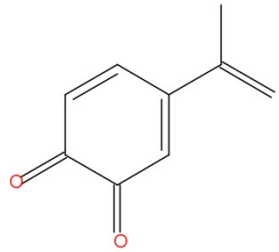	1,16
16.	C5	Maleic Acid	116	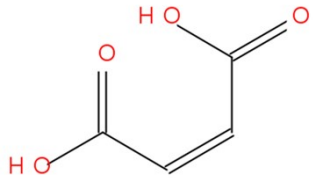	1

17.	D	4-Benzylphenol	199	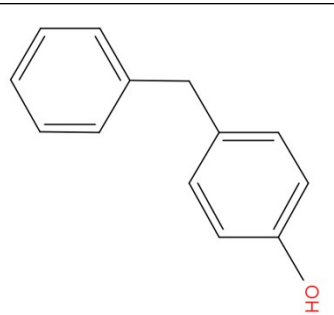	1,12
18.	D1	p-Hydroxybenzaldehyde	122	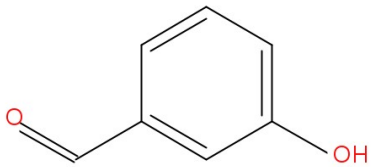	1,12
19.	D2	3,4-Dihydroxybenzoic acid	153	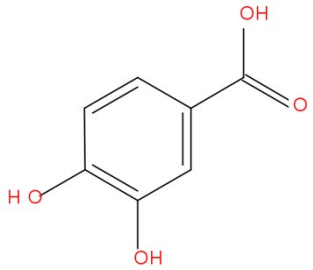	1,6,12
20.	E		241	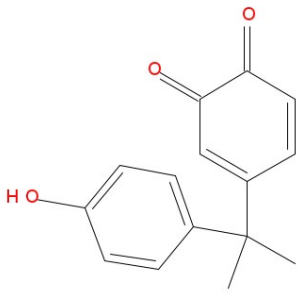	1,12

21.	F	2-Phenoxylcyclohexa-2,5-dienone	186	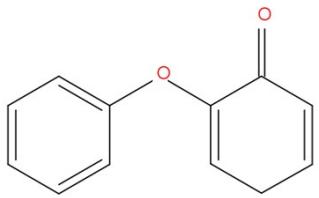	10
22.	G	[1,1'-Biphenyl]-4-ol	171	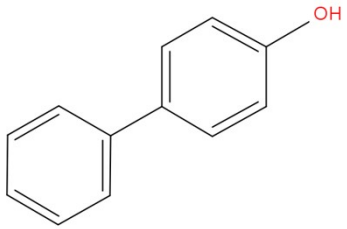	10
23.	H	o-Dihydroxybenzene (Catechol) (C6H6O2)	110	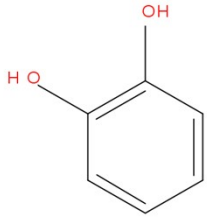	9
24.	I	Benzoquinone (C6H4O2)	108	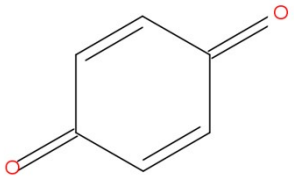	9
25.	J	[1,1'-Biphenyl]-4,4'-ol	186	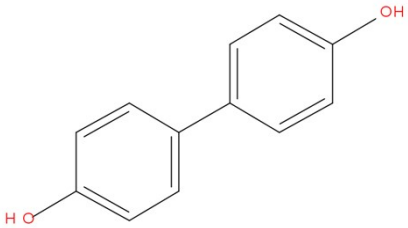	9

26.	K	Hydroxyl-hydroquinone	126	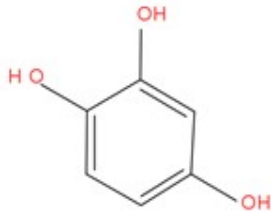	10
27.	K1	Hydroxyl-benzoquinone ``	124	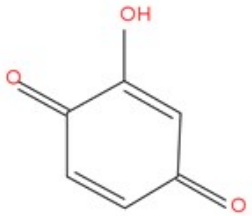	10
28.	L	3-Hydroxybenzaldehyde	122	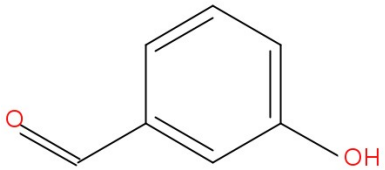	19
29.	M1a	2-Methylbenzene-1,4-diol	124	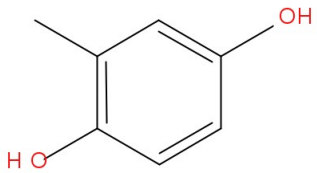	7
30.	M1b	3-Methylbenzene-1,2-diol	124	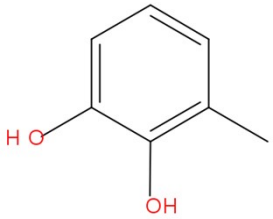	7

31.	M1c	4-Methylbenzene-1,2-diol	124	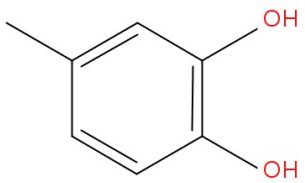	7
32.	M2	2-Methyl-p-benzoquinone	110	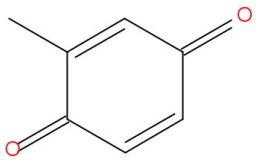	8
33.	L1	2,5-Dihydroxybenzaldehyde	138	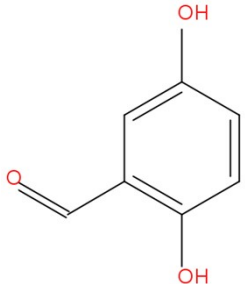	6,19
34.	Z1	2-Butanol	75	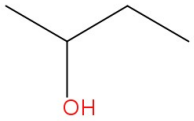	1
35.	Z2	Acrolein	56		10
36.	Z3	Glycerol	92	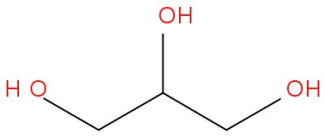	6,10
37.	Z4	Heptanoic acid	127	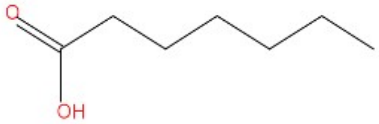	1

38.	Z5	Oxalic acid	90	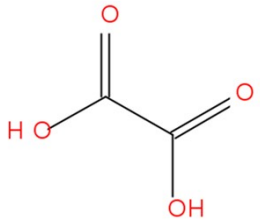	6,8
39.	Z6	Acetic acid	61	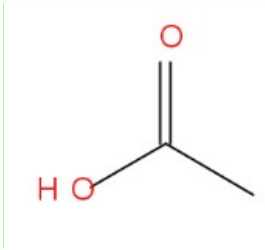	1
40.	Z7	Fumaric acid	116	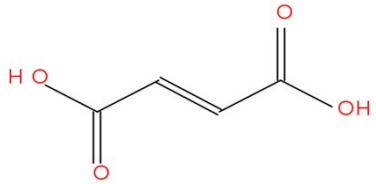	8,11,14
41.	Z8	Ethylene glycol	62	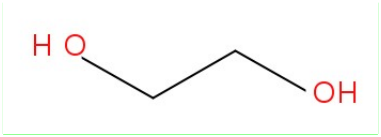	1,6
42.	Z9	Glycolic acid	77	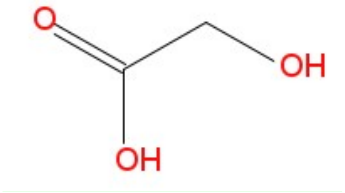	1,14

Table S5. Comparison of optimized Hematite/$Bi_4O_5I_2$ heterojunction nanocomposite with the existing heterojunction materials.

Heterojunction Catalysts	**Synthesis method**	**Light source**	**Catalyst dosage (g/L)**	**Phenolic compounds concentration (mg/L)**	**Degradation (%)/time (min)**
$Bi_7O_9I_3$–$Bi_4O_5Br_2$ [20]	Microwave oven	50 W LED lamp	0.1	BPA = 10	97.5/180
BiOCl/ZnCrZr-LBMO [21]	One-pot solvothermal	300 W Xe lamp	0.5	BPA = 10	94.2/60
$Bi_4O_5Br_2$/α-MnS [22]	Ball-milling processes	300 W Xe lamp	0.5	BPA = 20	78/180
BiOI/ZnO [23]	Solvothermal	300 W Xe lamp	0.2	BPA = 10	95/120
BiOI/Zn_2SnO_4 [24]	Oil bath	300 W Xe lamp	1.0	BPA = 20	99/180
g-C_3N_4/BiOI [25]	Solvothermal	50 W LED lamp	1.0	BPA = 20	90/120
β-CD/riboflavin @Bi_2WO_6 [26]	Hydrothermal	10 W Xe lamp	0.2	BPA = 10	95/40
$InVO_4$/Bi_5O_7I [27]	Hydrothermal and calcination	24 W LED lamp	0.04	BPA = 20	93.0/90
Co-$W_{18}O_{49}$/PDI [28]	Chemical preicipitation	250 W Xe lamp	0.5	BPA = 10	91.2/150

$AgBr/Ag/Bi_5O_7I$ [29]	Hydrothermal	500 W Xe lamp	0.4	BPA = 20	63/120
$Bi_4O_5I_2/Fe_3O_4$ [30]	Solvothermal	300 W Xe lamp	0.5	BPA = 20	89/80
$Fe_3O_4/BiOI$ [31]	Chemical precipitation	800W Xe lamp	1.0	BPA = 20	100/90
α-$MnO_2/Bi_7O_9I_3$ [1]	Chemical precipitation	50 W LED lamp	0.5	BPA = 20	97.5/80
V_2C/Bi_2WO_6 [32]	Hydrothermal	500 W Xe lamp	0.4	Phenol = 10	77.2/120
C@BiOBr [33]	Solvothermal	300 W Xe lamp	1.0	Phenol = 50	97/90
$Bi_4O_7/AgBiO_3$ [34]	Hydrothermal	300 W Xe lamp	0.5	Phenol = 20	74.87/120
$Bi_4O_5I_2/BiOCl$ [35]	Hydrothermal	300 W Xe lamp	0.5	Phenol = 10	100/180
$Co–Pd/BiVO_4$ [36]	Hydrothermal	300 W Xe lamp	0.8	Phenol = 20	90/180
Bi/COF [37]	Solvothermal	300 W Xe lamp	1.0	Phenol = 20	99/70
$N–Bi_2O_2CO_3/g\text{-}C_3N_4$ [38]	Hydrothermal	300 W Xe lamp	1.0	m-cresol = 25	97.29/180
Hematite/$Bi_4O_5I_2$ (This work)	**Chemical precipitation**	**50 W LED lamp**	**0.5**	**BPA = 20** **m-cresol = 20** **Phenol = 20**	**100/80** **100/80** **52.36/80**

Reference:

1 A. Rawat, S. K. Srivastava, C. S. Tiwary and A. K. Gupta, *J. Environ. Chem. Eng.*, 2024, **12**, 112879.

2 V. K. Parida, S. K. Srivastava, S. Chowdhury and A. K. Gupta, *Chem. Eng. J.*, 2023, **472**, 144969.

3 A. Majumder, A. Kumar, P. Sarathi and M. Varma, *J. Environ. Chem. Eng.*, 2021, **9**, 104812.

4 A. Majumder, A. K. Gupta and M. Sillanpää, *Colloids Surfaces A Physicochem. Eng. Asp.*, 2022, **648**, 129250.

5 Y. Zhang, E. K. Stefanakos and D. Yogi Goswami, *Build. Environ.*, 2013, **61**, 188–196.

6 Y. Chu, B. Miao, X. Zheng and H. Su, *Sep. Purif. Technol.*, 2021, **272**, 118866.

7 E. Zarei, *Int. J. Ind. Chem.*, 2018, **9**, 285–294.

8 Y. Chu, D. Zhang, L. Liu, Y. Qian and L. Li, *J. Hazard. Mater.*, 2013, **252**–**253**, 306–312.

9 L. Liu, H. Liu, Y.-P. Zhao, Y. Wang, Y. Duan, G. Gao, M. Ge and W. Chen, *Environ. Sci. Technol.*, 2008, **42**, 2342–2348.

10 T. T. T. Dang, S. T. T. Le, D. Channei, W. Khanitchaidecha and A. Nakaruk, *Res. Chem. Intermed.*, 2016, **42**, 5961–5974.

11 S. Zhang, H. Lan, Y. Cui, X. An, H. Liu and J. Qu, *Environ. Sci. Technol.*, 2022, **56**, 3552–3563.

12 Q. Wang, Y. Cao, Y. Yu, C. Zhang, J. Huang, G. Liu, X. Zhang, Z. Wang, H. Ozgun, M. E. Ersahin and W. Wang, *Chemosphere*, 2022, **308**, 136276.

13 A. Mondal, S. Sarkar and U. G. Nair, *Water Sci. Technol.*, 2021, **83**, 322–330.

14 T. Ahamad, M. Naushad, Y. Alzaharani and S. M. Alshehri, *J. Mol. Liq.*, 2020, **311**, 113339.

15 Y. Kanigaridou, A. Petala, Z. Frontistis, M. Antonopoulou, M. Solakidou, I. Konstantinou, Y. Deligiannakis, D. Mantzavinos and D. I. Kondarides, *Chem. Eng. J.*, 2017, **318**, 39–49.

16 X. Jiang, X. He, H. Huang, Y. Li, J. Yang, J. Mei and S. Cui, *J. Alloys Compd.*, 2023, **963**, 171221.

17 B. Kim, J. Jang and D. S. Lee, *Chemosphere*, 2022, **289**, 133040.

18 A. Garg, T. Singhania, A. Singh, S. Sharma, S. Rani, A. Neogy, S. R. Yadav, V. K. Sangal and N. Garg, *Sci. Rep.*, 2019, **9**, 765.

19 Y. Abdollahi, A. Zakaria and N. A. Sairi, 2014, **42**, 1292–1297.

20 A. Chachvalvutikul, T. Luangwanta, B. Inceesungvorn and S. Kaowphong, *J. Colloid Interface Sci.*, 2023, **641**, 595–609.

21 Y. Chen, D. Zhu, S. Xue, H. Wang, Q. Lu, G. Ruan, C. Zhao and F. Du, *Appl. Surf. Sci.*, 2024, **653**, 159337.

22 F. Chang, S. Zhao, Y. Lei, S. Peng, D. Liu and Y. Kong, *Sep. Purif. Technol.*, 2023, **304**, 122324.

23 C. Zhang, W. Fei, H. Wang, N. Li, D. Chen, Q. Xu, H. Li, J. He and J. Lu, *J. Hazard. Mater.*, 2020, **399**, 123109.

24 T. Yan, H. Liu, M. Sun, X. Wang, M. Li, Q. Yan, W. Xu and B. Du, *RSC Adv.*, 2015, **5**, 10688–10696.

25 J. Zhang, J. Fu, Z. Wang, B. Cheng, K. Dai and W. Ho, *J. Alloys Compd.*, 2018, **766**, 841–850.

26 Q. Lu, L. Di, Y. Zhou and Y. Zhou, *Sep. Purif. Technol.*, 2025, **353**, 128099.

27 Y. Li, Y. Li, L. Huang, S. Liu, M. Zhu, L. Qiu, J. Huang, Y. Fu and L. Huang, *J. Colloid Interface Sci.*, 2025, **677**, 234–249.

28 J. Liu, X. Gao, R. Wang, S. Zhu, X. Zhu, X. Zhu, D. Li, Q. Ruan, M. Cheng, B. Wang, H. Li, H. Xu and P. K. Chu, *Colloids Surfaces A Physicochem. Eng. Asp.*, 2024, **703**, 135050.

29 H. Ding, Y. Guan, Z. Wang, Y. Yamauchi, Y. Asakura and Q. Han, *J. Alloys Compd.*, 2024, **1002**, 175215.

30 F. Chang, H. Chen, X. Zhang, B. Lei and X. Hu, *Sep. Purif. Technol.*, 2020, **238**, 116442.

31 S. Gao, C. Guo, J. Lv, Q. Wang, Y. Zhang, S. Hou, J. Gao and J. Xu, *Chem. Eng. J.*, 2017, **307**, 1055–1065.

32 K. Li, J. Zhu, W. Zhou, L. Sun and S. Tian, *Ceram. Int.*, 2024, **50**, 23694–23709.

33 Z. Han, Y.-G. Liu, R. Zhang, J. Shi, Y. Jia, X. Liu and H.-Y. Jiang, *Langmuir*, , DOI:10.1021/acs.langmuir.4c01829.

34 Z. Jia, J. Liu, R. Li, C. Fan and Y. Wang, *Mater. Sci. Semicond. Process.*, 2024, **177**, 108359.

35 Y. Zhong, C. Wu, D. Chen, J. Zhang, Y. Feng, K. Xu, W. Hao, H. Ding, G. Lv, Y. Du and L. Wang, *Appl. Catal. B Environ.*, 2023, **329**, 122554.

36 S. Wang, H. Luo, X. Xu, Y. Bai, X. Song, J. Zhang, J. Li, J. Zhao and C. Tang, *Surfaces and Interfaces*, 2016, **5**, 39–46.

37 S.-H. Ma, W.-L. Jin, W. Li, H.-Y. Wang, L.-N. Zhu, M. Zeng and D.-M. Kong, *ACS Appl. Nano Mater.*, 2023, **6**, 14151–14164.

38 Y. Huang, M. Li, X. Zhang, B. Xing, Y. Ye and Y. Zeng, *Environ. Res.*, 2024, **242**, 117771.

Revised supplementary Figures

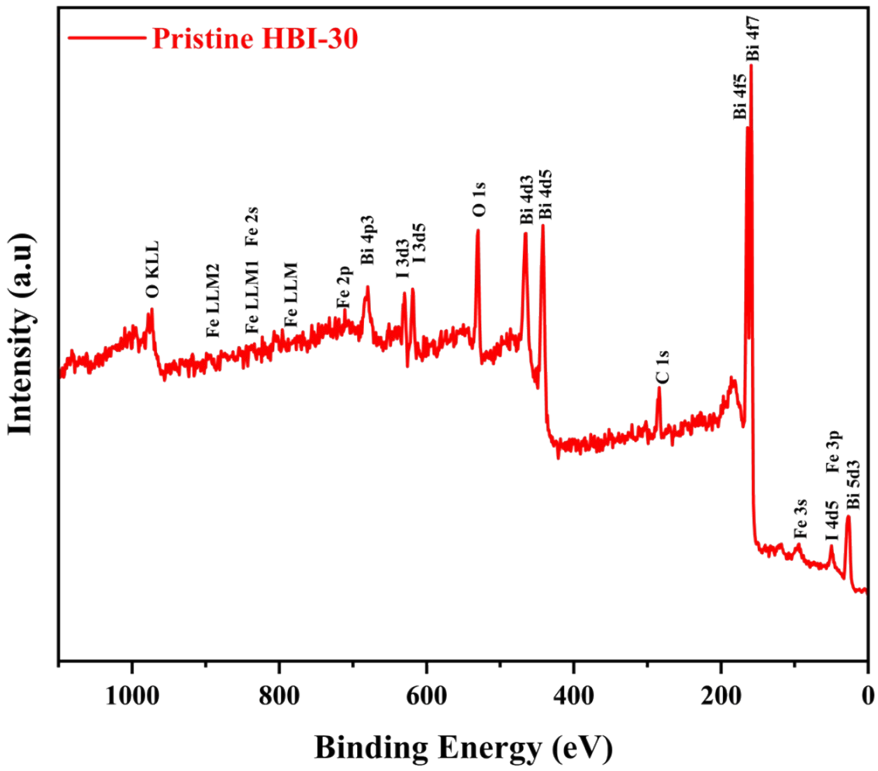

Fig. S1. XPS survey spectrum of HBI-30.

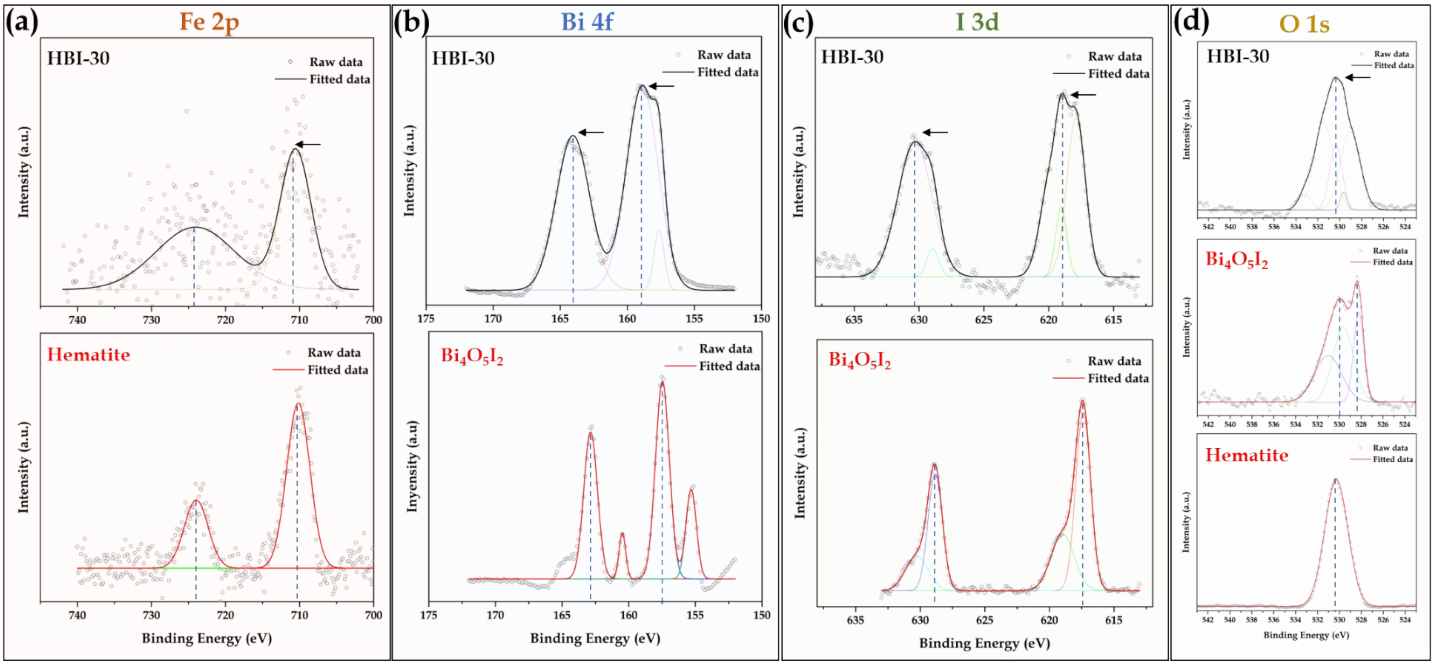

Fig. S2. XPS Comparison of pristine (Hematite and $Bi_4O_5I_2$) with HBI-30 composite, (a) Fe 2p, (b) Bi 4f, (c) I 3d, and (d) O 1s.

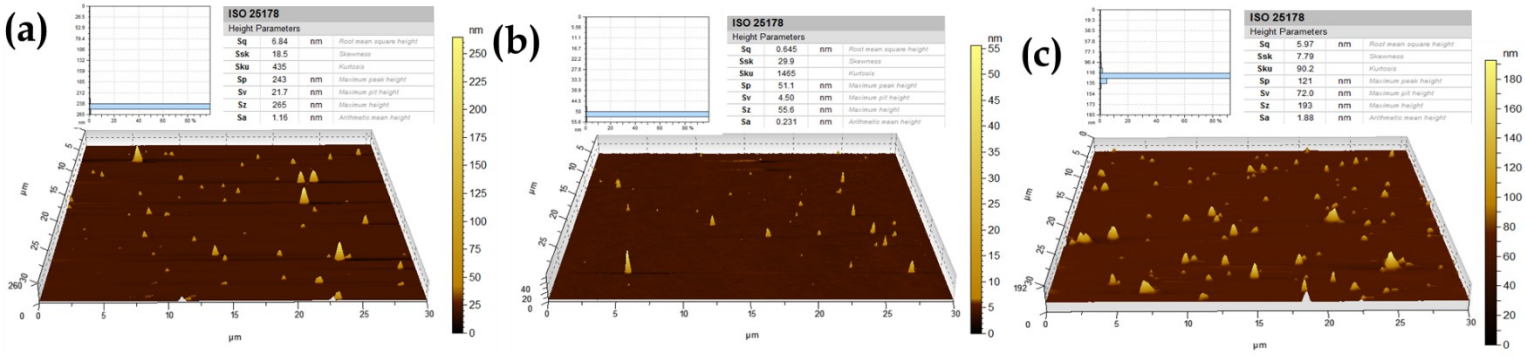

Fig. S3. AFM 3D topology of (a) hematite, $Bi_4O_5I_2$, HBI and inset of each Fig. (a-c) histogram and height parameters of hematite, $Bi_4O_5I_2$, and HBI-30.

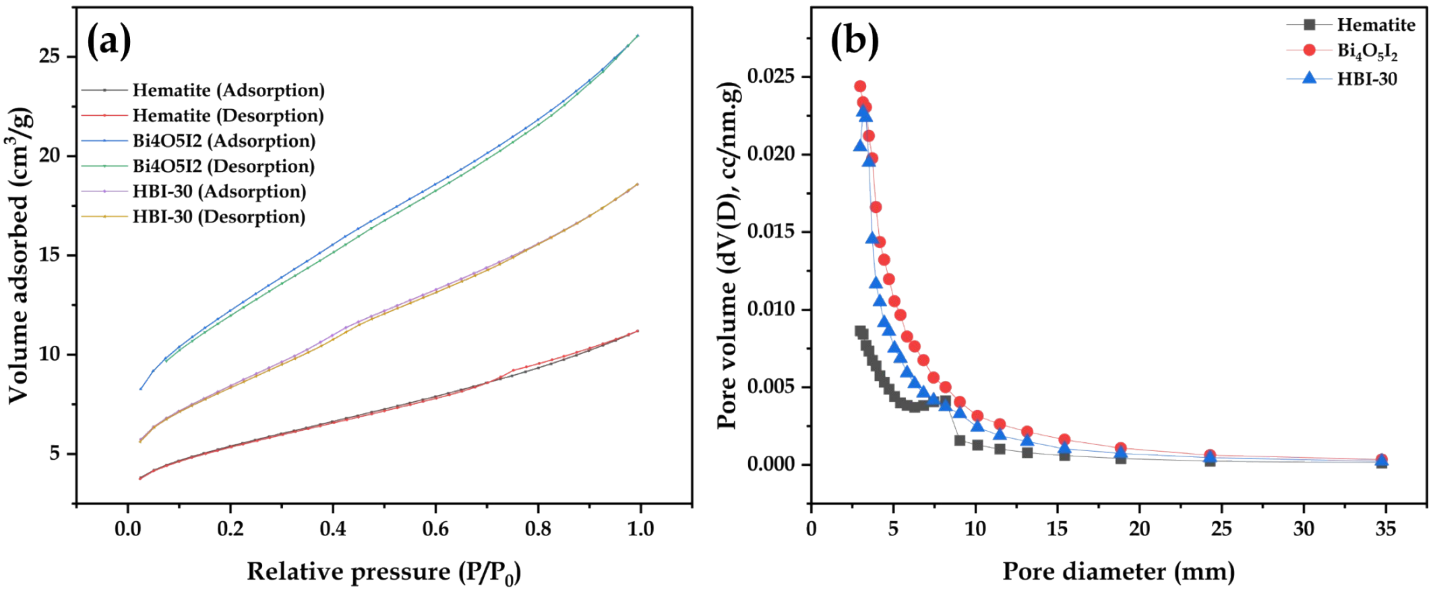

Fig. S4. (a) N_2 adsorption/desorption isotherms, and (b) pore size distribution curves for Hematite, $Bi_4O_5I_2$, and HBI-30.

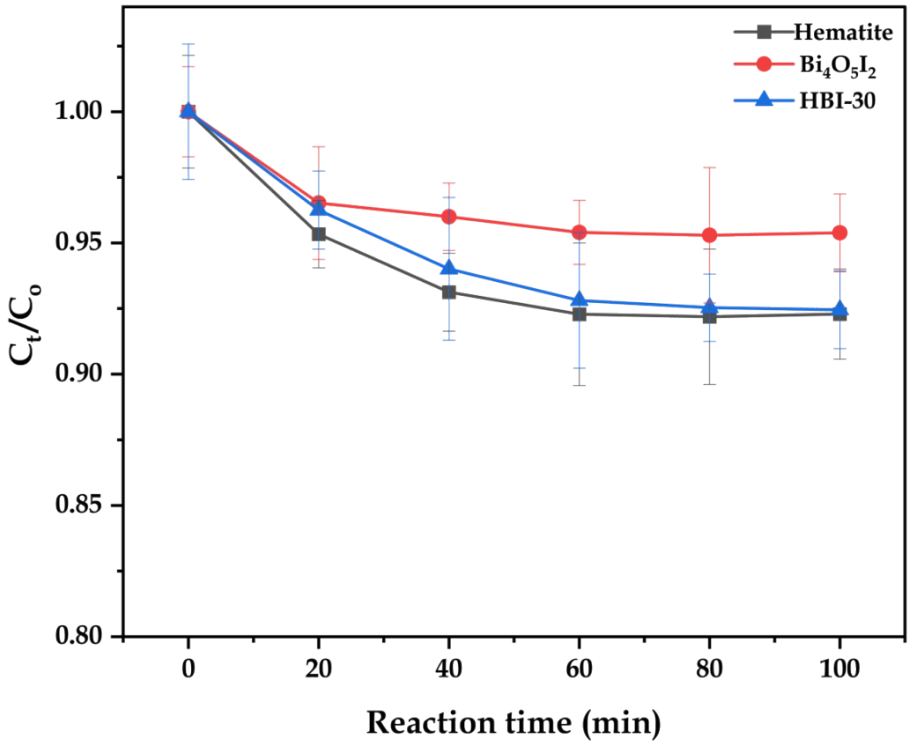

Fig. S5. (a) Adsorption/desorption of BPA (10 mg/L) on Hematite, $Bi_4O_5I_2$, andf HBI-30.

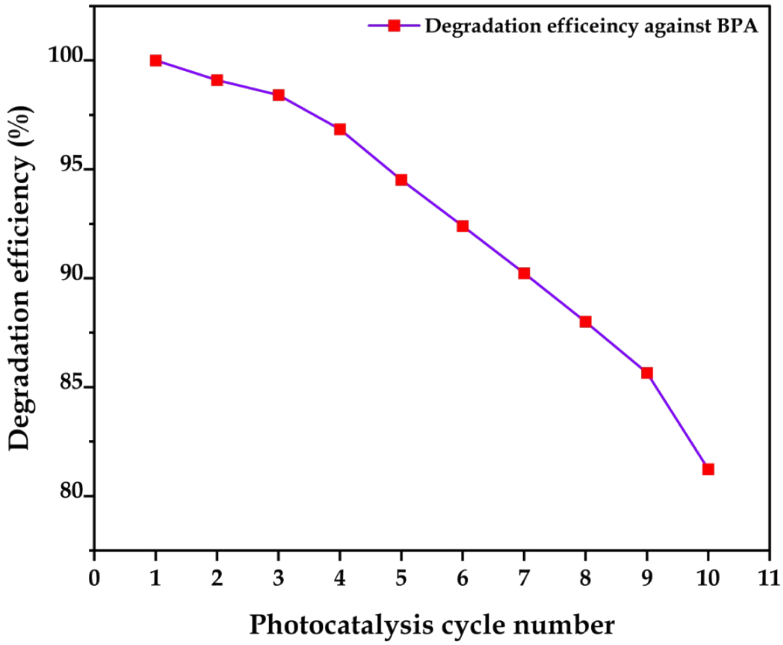

Fig. S6. Reusability test of HBI-30, up to ten cycles.

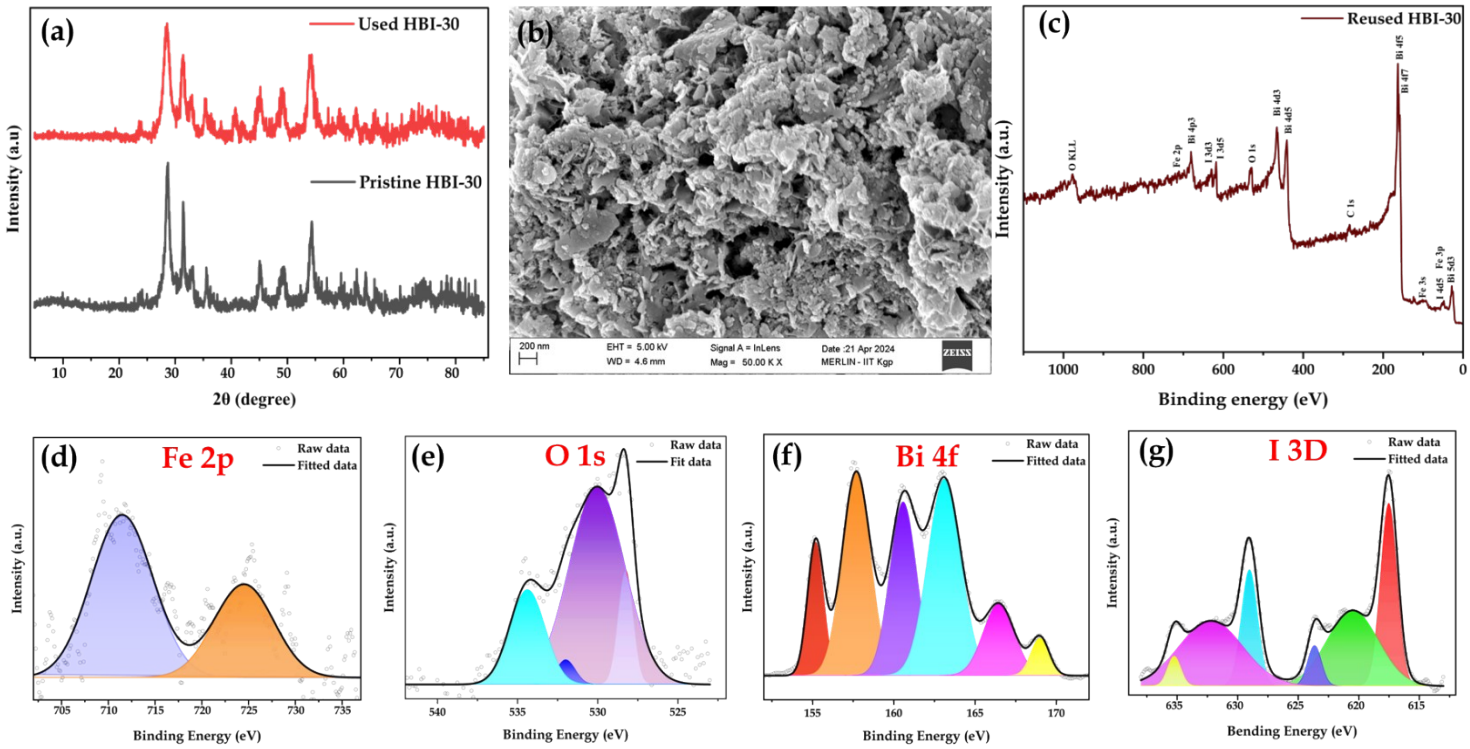

Fig. S7. (a) XRD pattern of unused and reused HBI-30, (b) FEG-SEM image and (c) XPS survey scan of reused HBI-30, and deconvoluted XPS spectra for (d) Fe 2p, (e) O 1s, (f) Bi 4f, and (g) I 3D.

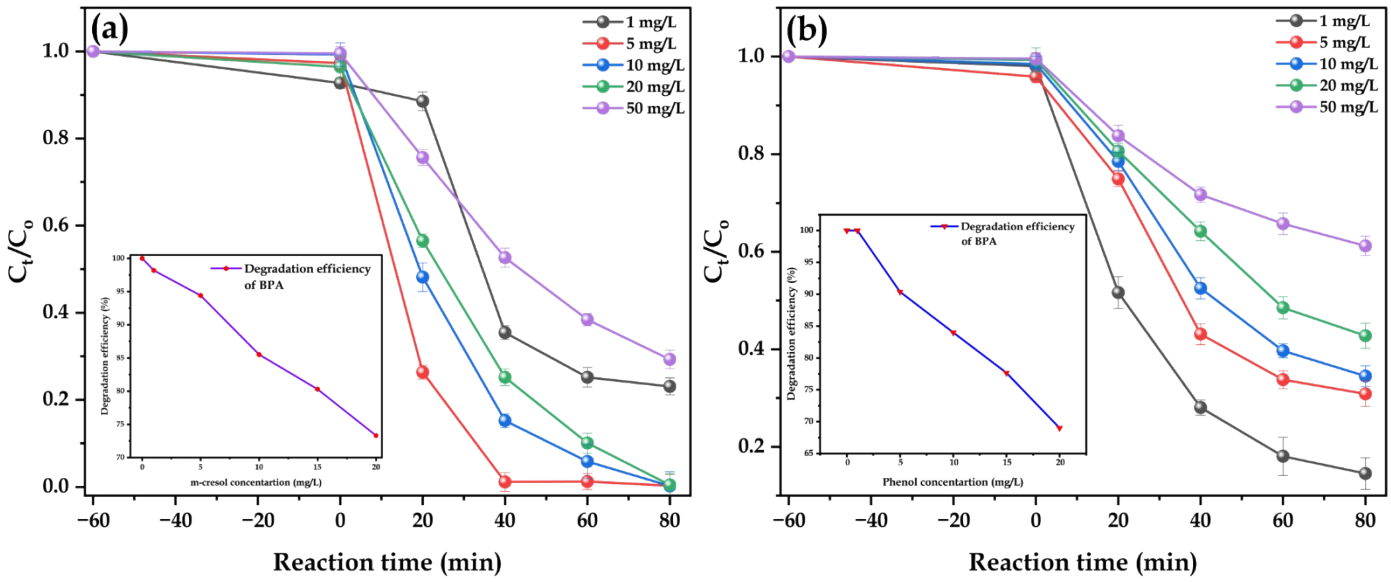

Fig. S8. Photocatalytic degradation of (a) m-cresol and (b) phenol, with insets showing the effect of their varying concentrations on BPA degradation efficiency.

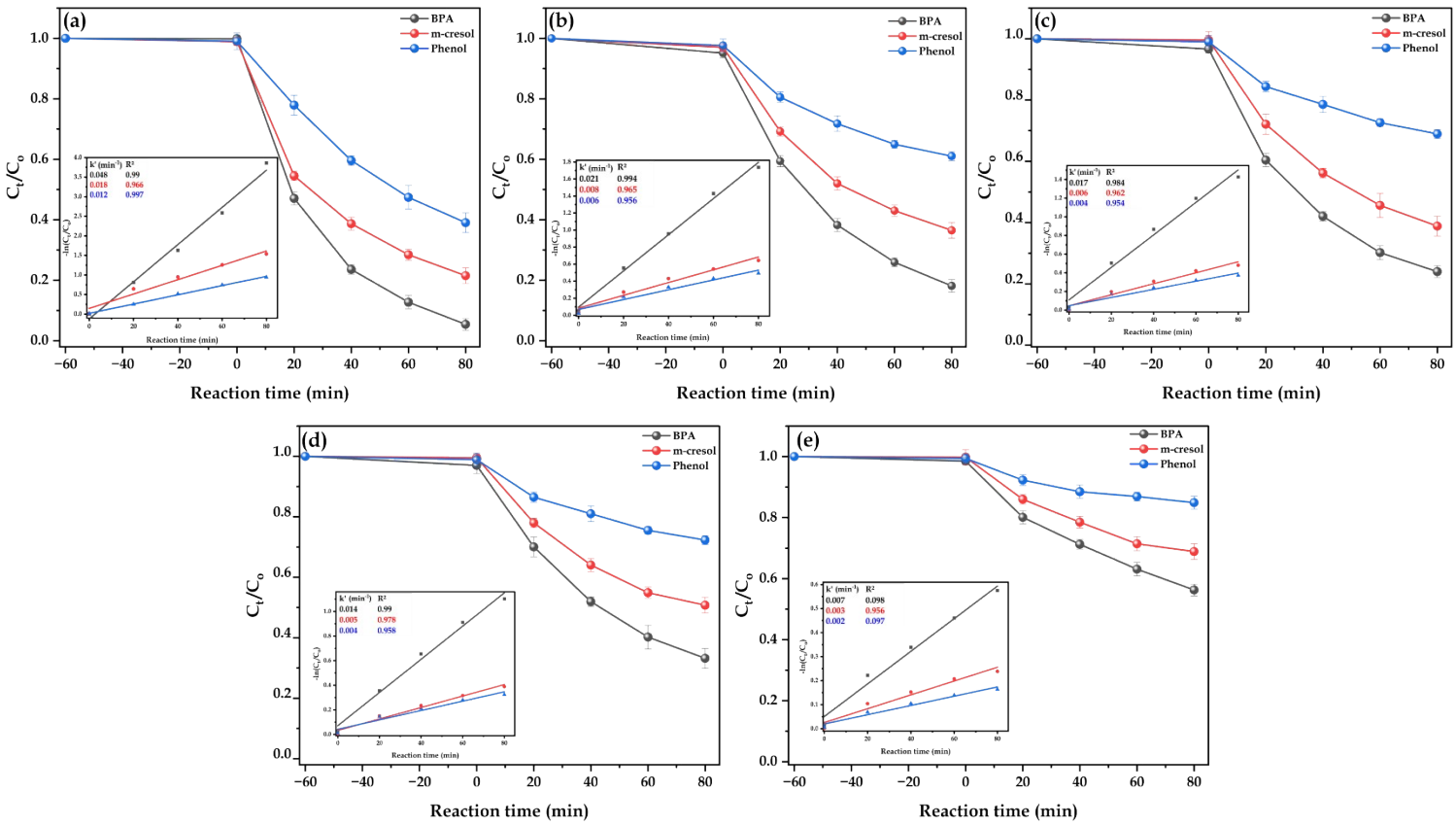

Fig. S9. Simultaneous degradation of phenolic compounds in different water matrices, (a) DI water, (b) tap water, (C) river water, (d) pond water, and (e) secondary effluent of the wastewater treatment plant, with inset of kinetic model for respective figures.

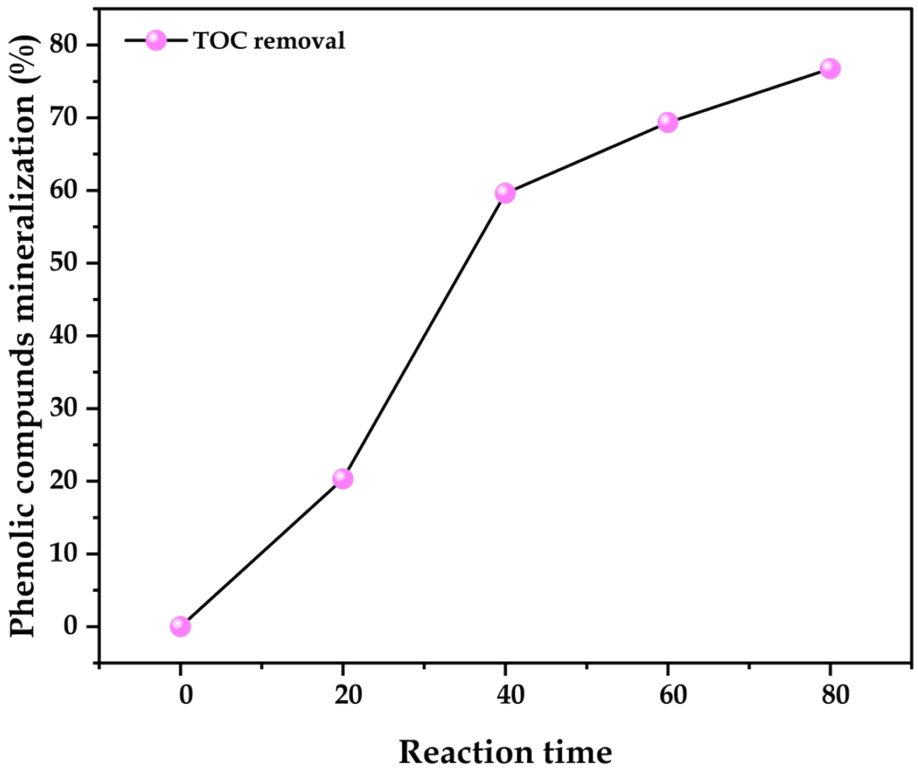

Fig. S10. TOC removal under operatoinal parameters: initial concentration of BPA, m-cresol, and phenol is 10, 5, and 5,mg/L respectively; catalyst dose = 0.5 g/L; pH = 6.75.

(a)

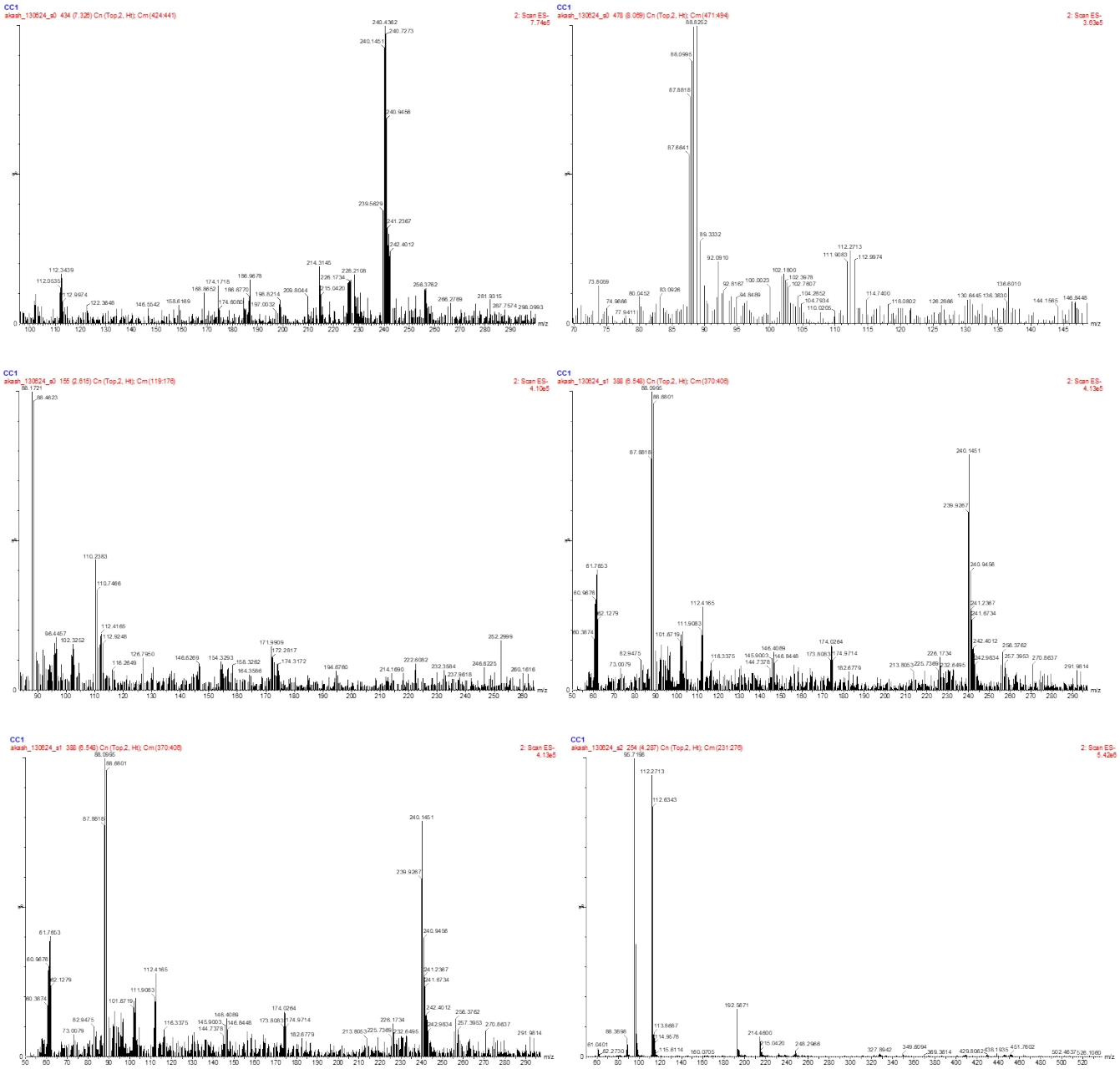
CC1
akash_130624_s0 434 (7.328) Cn (Top,2, Ht); Cm (424:441)
2: Scan ES-
7.74e5
CC1
akash_130624_s0 478 (8.069) Cn (Top,2, Ht); Cm (471:494)
2: Scan ES-
3.63e5
CC1
akash_130624_s0 155 (2.615) Cn (Top,2, Ht); Cm (119:176)
2: Scan ES-
4.10e5
CC1
akash_130624_s1 388 (6.548) Cn (Top,2, Ht); Cm (370:406)
2: Scan ES-
4.13e5
CC1
akash_130624_s1 388 (6.548) Cn (Top,2, Ht); Cm (370:406)
2: Scan ES-
4.13e5
CC1
akash_130624_s2 254 (4.287) Cn (Top,2, Ht); Cm (231:276)
2: Scan ES-
5.42e6
%
m/z

(b)

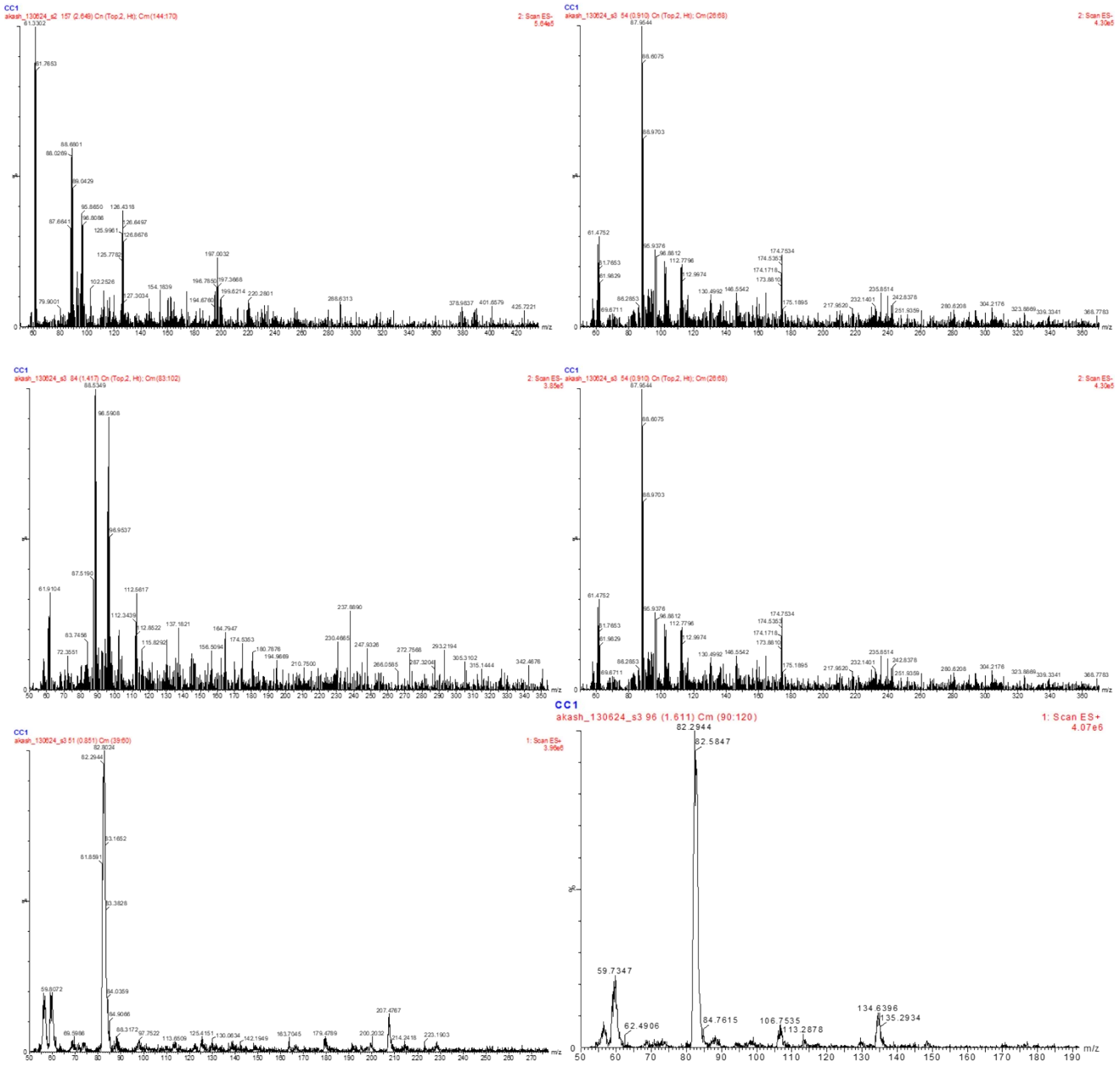

Fig. S11b. LC-MS/MS-identified peaks of degradation products after photocatalytic degradation of phenolic compounds (Part II/III).

(c)

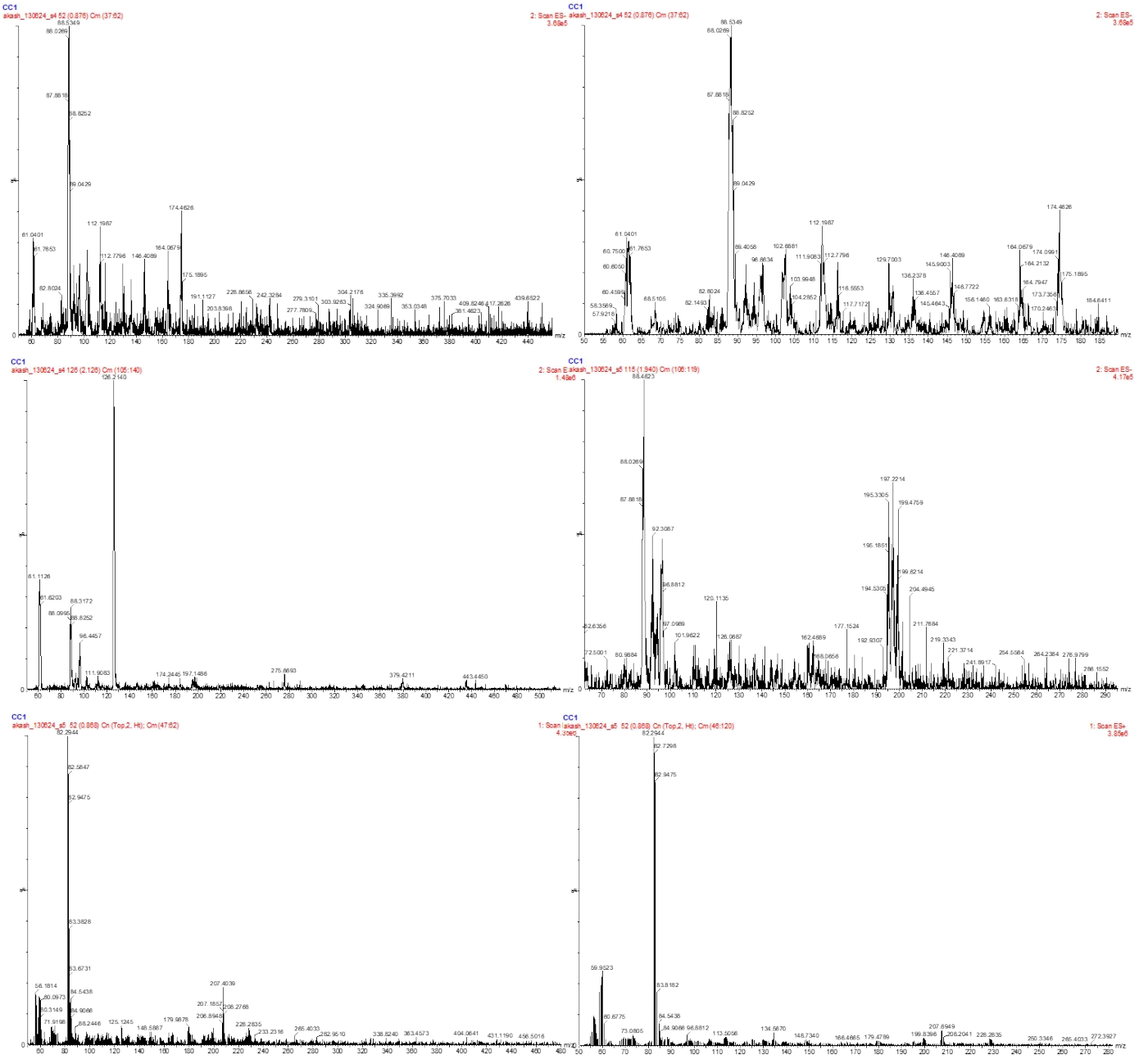

Fig. S11c. LC-MS/MS-identified peaks of degradation products after photocatalytic degradation of phenolic compounds (Part III/III).

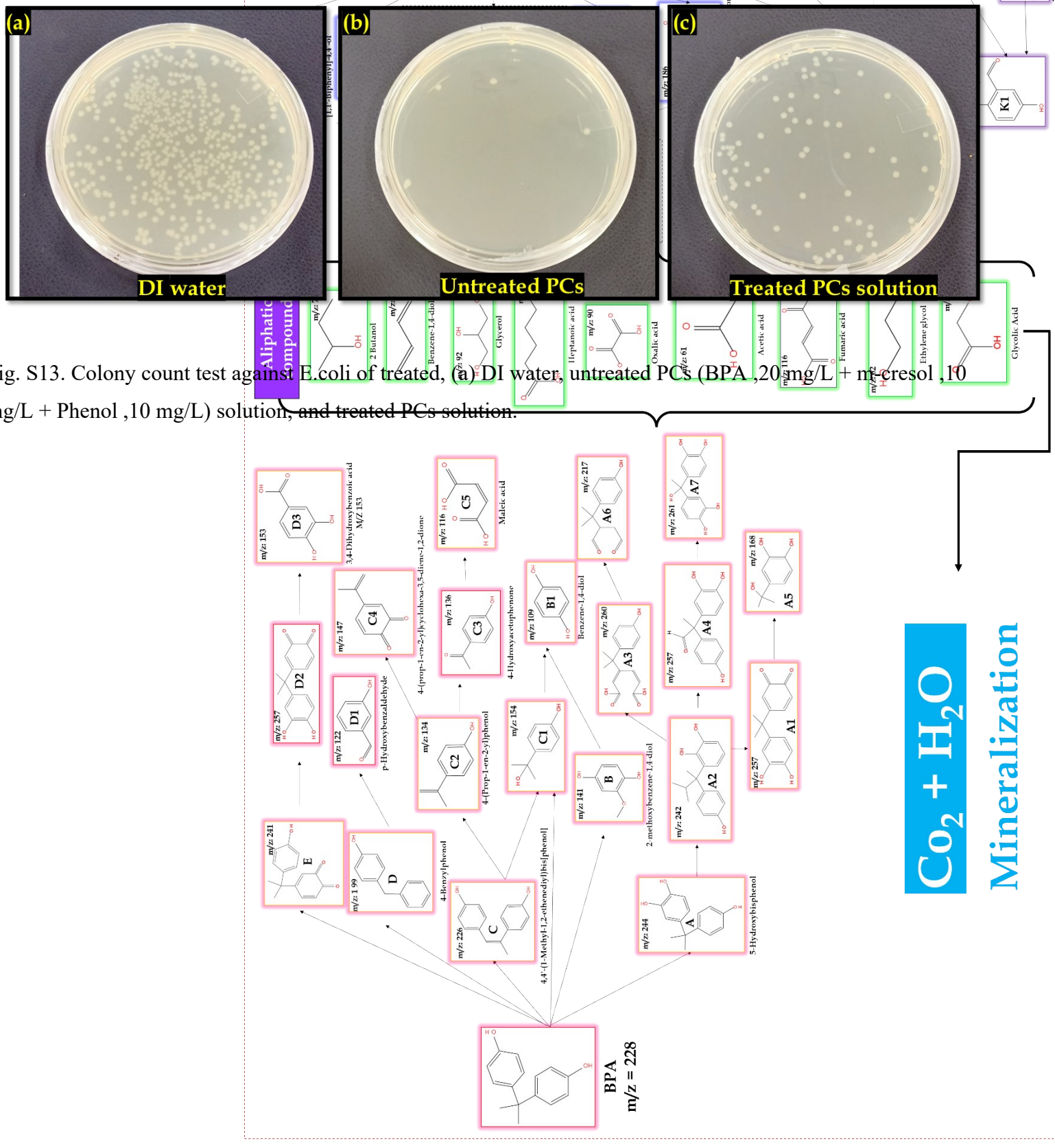

Fig. S13. Colony count test against E.coli of treated, (a) DI water, untreated PCs (BPA ,20 mg/L + m-cresol ,10 mg/L + Phenol ,10 mg/L) solution, ~~and treated PCs solution.~~

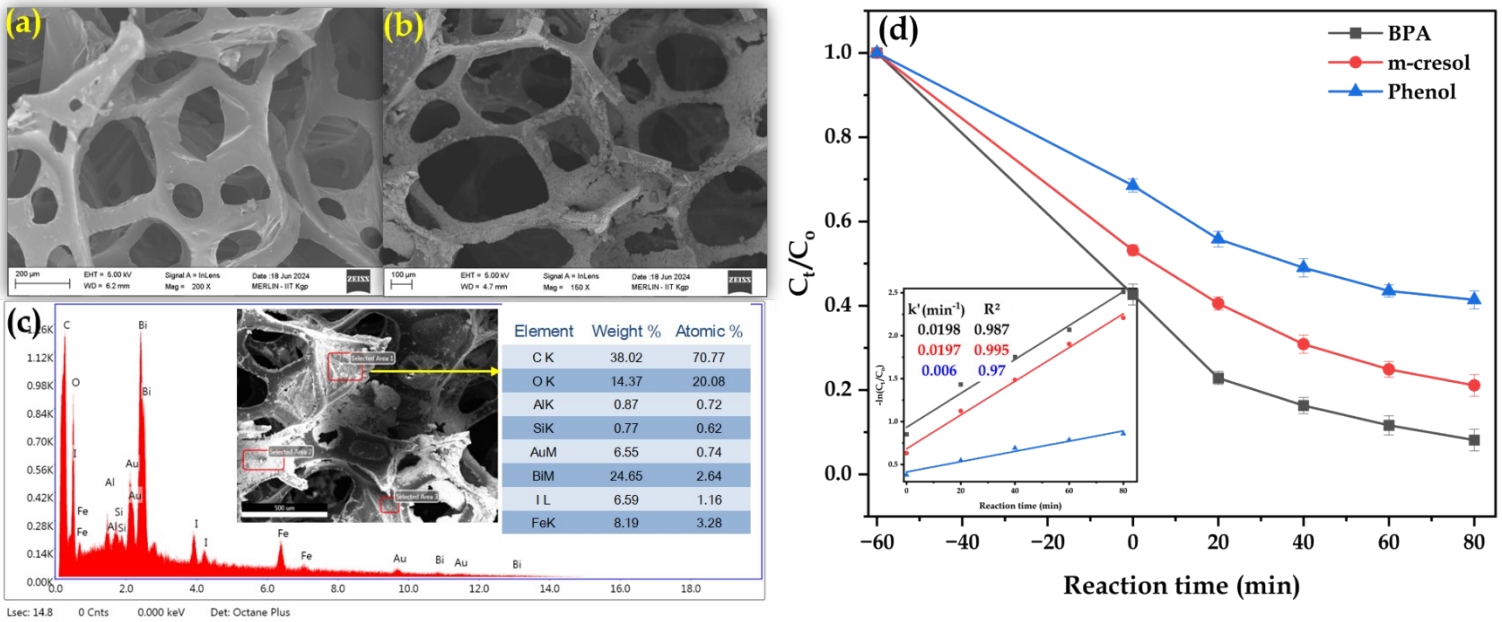

Fig. S14. FEG-SEM image of (a) pristine and (b)coated PU foam, (c) XRD pattern of unused and reused HBI-30, (b) FEG-SEM image of reused HBI-30, (c) EDAX analysis of HBI@PU, and (d) simultaneous degradation of phenolic compounds.